Examining phase contrast sensitivity to signal location and tissue thickness in breast imaging

Stefano Vespucci, Cale Lewis, Chan Soo Park, Mini Das

Stefano Vespucci, Cale Lewis, Chan Soo Park, Mini Das, "Examining phase contrast sensitivity to signal location and tissue thickness in breast imaging," Proc. SPIE 10573, Medical Imaging 2018: Physics of Medical Imaging, 1057324 (9 March 2018); doi: 10.1117/12.2294968

SPIE.

Event: SPIE Medical Imaging, 2018, Houston, Texas, United States

Examining phase contrast sensitivity to signal location and tissue thickness in breast imaging

Stefano Vespucci[a], Cale Lewis[a], Chan Soo Park[a] and Mini Das[a,b]

[a]Department of Physics
[b]Department of Biomedical Engineering
University of Houston, Houston, TX 77204

ABSTRACT

X-Ray phase contrast imaging (PCI) is being developed as an alternative to overcome the poor contrast sensitivity of existing attenuation imaging techniques. The "phase sensitivity" can be achieved using a number of phase-enhancing geometries such as free space propagation, grating interferometry and edge illumination (also known as coded aperture) technique. The enhanced contrast in the projected intensities (that combine absorption and phase effect) can vary by object shape, size and its material properties as well as the particular PCI method used. We show a comparison of this signal enhancement for both FSP and coded aperture (CA) PCI. Our data shows that the phase enhancement is significantly higher for CA in comparison to FSP. Our preliminary results indicate that the enhanced phase effect decreases in all PCI techniques with increasing background thickness. Investigations involving signal location and background tissue thickness dependent signal enhancement (and/or loss of this signal) are very important in determining the true benefit of PCI methods in a practical application involving thick organs like breast imaging.

Keywords: X-ray, Medipix, Phase contrast imaging, Computerized tomography

1. INTRODUCTION

Since Röntgen's discovery, x-ray imaging and the possibility to "see" through objects, has found application is a large number of fields such as product inspection, security, material science etc. In medical imaging, x-ray based imaging techniques are considered one of the most important diagnosis tools. For over a century, x-ray imaging has only been based on sample's x-ray attenuations. However, it is difficult to discriminate soft tissue types with very similar attenuation properties.

X-rays phase contrast imaging methods have been investigated to explore the wave properties of x-rays, yielding additional information as they refract when they travel through objects.[1–8] In biological tissues this "phase effect" can be several order of magnitude higher than absorption.[9] The magnitude of phase change introduced by an object is determined by its refractive index.[1] The x-ray complex refraction index, n, can be written as

$$n = 1 - \delta + i\beta, \tag{1}$$

where δ is the refractive index decrement responsible for x-ray phase shift and β is the imaginary part of n, which is responsible for the x-ray absorption. For soft tissue, δ can be approximated as

$$\delta = \frac{r_e \lambda^2}{2\pi} \rho_e \approx 4.49 \times 10^{-16} \lambda^2 \rho_e \tag{2}$$

where ρ_e is the electron density. The magnitude of phase shift

$$\phi = -\frac{2\pi}{\lambda} \int \delta(s) ds, \tag{3}$$

Author for correspondence :
Mini Das: E-mail: mdas@uh.edu

Medical Imaging 2018: Physics of Medical Imaging, edited by Joseph Y. Lo, Taly Gilat Schmidt, Guang-Hong Chen, Proc. of SPIE Vol. 10573, 1057324
 · doi: 10.1117/12.2294968

where the integral is over the x-ray path.

Phase-based tissue contrast can be revealed in several ways. X-ray phase contrast imaging (PCI) methods include x-ray interferometry, diffraction-enhanced imaging (DEI), coded aperture and in-line (or free space propagation) phase contrast imaging. Because of the simplicity of the experimental set-up, this work examines free space propagation and coded aperture PCI techniques.

For both in-line and coded aperture phase-contrast imaging, monochromaticity of the source is not a stringent requirement.[10,11] It has been shown that in-line and coded aperture phase-contrast imaging provides unprecedented details from biological tissue. Within the diagnostic x-ray energy range, δ is more than three order of magnitude higher than β. Additionally, δ decreases slower than β as the energy increases. This could potentially create new low dose imaging approaches. Phase-contrast imaging, thus, opens up new possibilities in a number of clinical applications[12] where attenuation based x-ray imaging is somewhat limited. These include cartilage bone, blood vessels, breast, lung, renal and prostate carcinoma imaging.[9,13]

This work shows a systematic study of the variation in the phase-contrast signal under different PCI experimental geometries: free-space propagation and coded aperture (CA) PCI.[11,14] The dependence of signal location and tissue thickness on the detected phase enhanced signal is also investigated. These investigations are important in determining the true benefits of PCI method in a practical application involving thick organs like breast imaging.

A schematic of the FSP and CA PCI are shown in Fig. 1. For FSP, increasing the propagation distance past the object plane enhances the phase signal which can then be detected via available detectors. In a CA geometry, the refraction of the beamlets created by a first mask (object mask) is allowed to be recorded by placement of suitable second x-ray mask at the detector. While a higher degree of spatial coherence is important in FSP, these conditions are relaxed for a CA setup. The signal formation in the projected PCI image for both configurations can be intuitively understood via the corresponding transport of intensity (TIE) equations 4 and 5,[15–17]

$$I_{R_2} = \frac{I_{R_1}}{M^2}(1 - \frac{R_2}{Mk(E)}\nabla^2\phi) \;\; for\ FSP \tag{4}$$

$$I_{R_2} = \frac{I_{R_1}}{M^2}(1 - \frac{R_2}{Mw_e k(E)}\nabla\phi) \;\; for\ CA. \tag{5}$$

where $M = \frac{R_1+R_2}{R_1}$ is the magnification factor, $k(E)$ is the wave-vector and w_e is the relative mask displacement. These equations can also allow efficient phase retrieval.

While the TIE for a FSP was well understood as shown in Eq. 4, the TIE for an EI was derived recently as shown in Eq. 5.[15,16] For a given energy, the sensitivity of FSP to the phase variations can be enhanced due to propagation distance R_2 while in a CA PCI, both the relative mask displacement w_e and propagation distance R_2 can contribute to this enhancement.

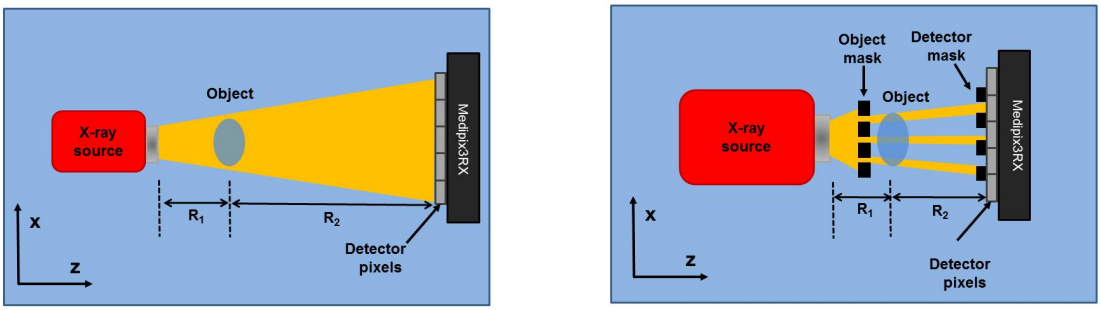

(a) (b)

Figure 1: Top view of the schematic of a (a) FSP PCI and (b) EI PCI set up.

2. METHODS

A benchtop FSP and CA PCI setup is constructed in our laboratory along with PCI CT setup. The setup for CA PCI has been automated for faster alignment and data acquisition. In this work we show results obtained with a micro-focus x-ray tube L8121-03 from Hamamatsu capable of up to 150 kV and 500 μA using Tungsten cathode with focal spot size ranging from 7 to 20 μm. No filter was used to harden the x-ray beam. The masks currently available for the coded aperture PCI set-up have a thickness of gold stripes of 125 μm allowing blocking of 40 keV x-rays to only 96%. A Medipix3RX[18–20] detector with 55m pitch and 1000 μm thick CdTe sensor was used. The detector was used in an energy integrating mode for these studies without exploring its spectral capabilities.

For the free space propagation PCI experiments, the source to detector distance was set to 2 m. A number of source to object distances were used, in order to find the optimal condition; this procedure is described in detail in the next section. For the coded aperture experiment, the source to object mask, the source to detector mask and the source to detector distances were set to 74, 106 and 110 cm respectively. The chosen propagation distance (36 cm) for CA setting was decided by the specifications of the mask pairs currently available in our laboratory. The only adjustable parameter in this case was the relative masks displacement (w_e).

For both FSP and CA settings the enhancement of phase contrast depends on the energy and on the propagation distance (R_2); for CA there is a further dependence on the mask displacement w_e (as described by the Eq. 5). To examine the relative enhancement of a given signal for FSP and CA methods, signal enhancement was tested using a cylindrical PMMA rod of diameter 6.4 mm embedded in various locations in both anthropomorphic breast phantom slices of varying thickness from CIRS Inc. as well as in PMMA slabs. The edge enhancement was calculated by

$$Edge\ enhancement\ (\%) = \frac{I_{max} - I_{ff}}{I_{ff}} \times 100, \tag{6}$$

where I_{max} and I_{ff} refer to the maximum and flat field intensity measured from the average PMMA rod intensity profile respectively (see also Fig. 2).

3. OPTIMIZATION OF THE EXPERIMENTAL SET-UP

3.1 Free Space Propagation

An initial optimization of the experimental set-up was carried out. The best imaging geometry was determined experimentally, by determining the combination of R_1 and R_2 values where edge enhancement from the signal was maximum. In general, according to Eq. 4, for a fixed photon energy and source-to-object distance, an increase in the phase-contrast enhancement is expected when increasing the propagation distance R_2. However, in a

practical situation where the source-to-detector distance is fixed (in a clinical imaging system for example), an increase in the propagation distance involves a decrease of the source-to-object distance R_1. This leads to reduced lateral coherence and higher geometric blurring. Hence the optimization consists in finding the optimal R_1 and R_2 values that maximize both spatial coherence of the source and propagation distance. In our experiments, a peak energy of 40 keV, 250 μA current and a 7 μm source size was used. By fixing source-to-detector distance to 2m, the position of the sample (R_1) was varied at regular 0.1 m intervals at intermediate positions between the source and the detector. The optimal geometry was determined by evaluating the edge enhancement from the PMMA rod, as shown in Fig. 2.

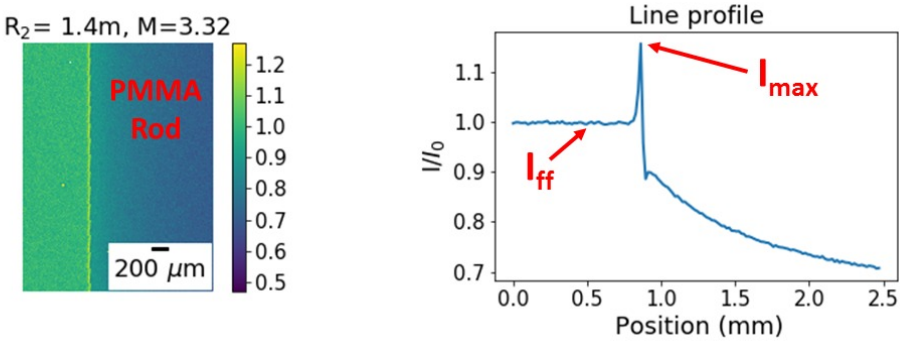

(a) (b)

Figure 2: Edge enhancement from an PMMA rod obtained in FSP geometry. (a) Image acquired by using a focal spot size of 7 μm, a x-ray tube peak energy of 40 keV, a propagation distance of 1.4 m and a $\times$ 3.32 magnification. (b) Mean profile obtained by averaging the image along the vertical direction.

The edge enhancement measured as function of R_2 is shown in Fig. 3. Edge enhancement is optimal when the propagation distance is in the 1.35 m - 1.6 m range. When the propagation distance in above the optimal range, the reduced spatial coherence deteriorates the phase contrast effects.

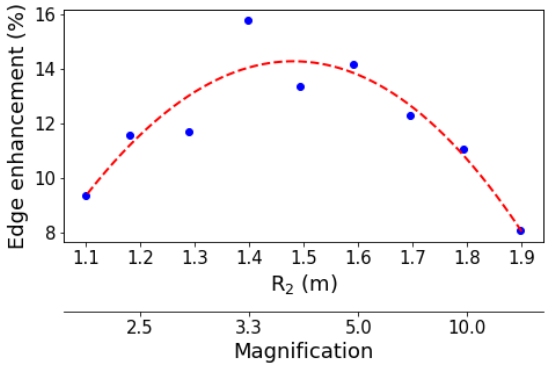

Figure 3: FSP PCI geometry optimization. PMMA rod edge enhancement for different R_2 and corresponding magnification values. R_1 values were changed accordingly, so as to have $R_1 + R_2 = 2$ m. All images were acquired by using a focal spot size of 7 μm, a x-ray tube peak energy of 40 keV.

Setting the propagation distance to 1.4 m, corresponds to a magnification of approximately $\times$3.3, resulting in an edge enhancement from the PMMA rod that is of the order of 14%. This optimized FSP geometry is maintained fixed throughout the remaining FSP experiments presented in this paper.

Figure 4: Example of FSP PCI from a dry wasp.

An example of FSP PCI application to a biological specimen, a dry wasp, is shown in Fig. 4. Phase contrast enhancements are visible at all interfaces between tissues: exoskeleton, wings and muscles are all enhanced. Details of the internal structure are clearly discernible.

3.2 Coded aperture

A preliminary optimization was also carried out for the coded aperture geometry. As mentioned before, unlike FSP, the geometrical arrangement for coded aperture is fixed by the mask dimensions. The optimization procedure consisted in evaluating optimal photon energy and masks displacement. Preliminary beam visibility tests have shown visibility of the signal increasing when decreasing beam energy. This is attributed to masks thickness (125 μm), not being sufficient to fully absorb high-energy photons. Since mask absorption increases by decreasing the photon energy, a more ideal mask behavior is obtained by exploiting low energy photons. An x-ray tube peak energy of 40 keV energy was found to be sufficiently low to allow up to 96% of photons to be absorbed. A low w_e increases edge enhancement at the expense of reduced photon flux. A mask displacement effect was evaluated by measuring the edge enhancement from the PMMA rod as function of the displacements. This is shown in Fig. 5, where the normalized measured photon intensities are also shown. For a mask displacement of approximately 6.27 μm, an edge enhancement value is of the order of 60% was observed. This is much larger than the 14% enhancement obtained in FSP.

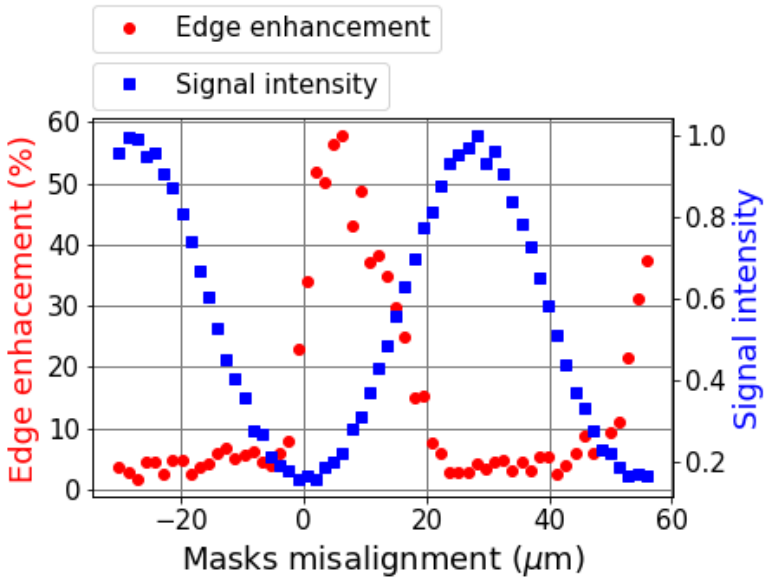

Figure 5: CA PCI geometry optimization. PMMA rod edge enhancement for different w_e values (left y-axis). The right y-axis shows the corresponding normalized signal intensities.

4. INVESTIGATING CHANGE IN PCI SIGNAL ENHANCEMENT DUE TO SIGNAL LOCATION IN THE OBJECT.

In the previously presented experiments, x-rays from the signal (PMMA tube) was freely propagating towards the detector. In a real application, the object of interest is often embedded within a thicker sample; this is often the situation found in clinical applications, for example in mammography. There are still debates on the actual effectiveness of phase-contrast techniques when applied to thick specimens.

To determine whether the edge enhancement produced by a signal is detectable when photons further propagate through additional material thickness, five breast phantom slices (CIRS anthropomorphic breast phantom), each of 1 cm thick, were placed before or after the rod in two different experiments. The result is shown in Fig. 6. Figure 6(a) shows the signal without any additional background thickness; Figs.6(b-c) show the signal degradation when 5 cm of breast phantom is placed before and after the signal respectively. Although a reduction in the edge enhancement is visible, the phase contrast effect is still sufficiently large to allow a clear identification of the PMMA rod edge. Edge enhancement degradation in both configurations is of the same order of magnitude, i.e. phase contrast degradation does not significantly depend on the position of the signal within the thicker object. Because the breast phantom texture locally affects the signal enhancement, a quantitative measurement of the signal degradation has been performed by using PMMA slabs, which has a more homogeneous texture.

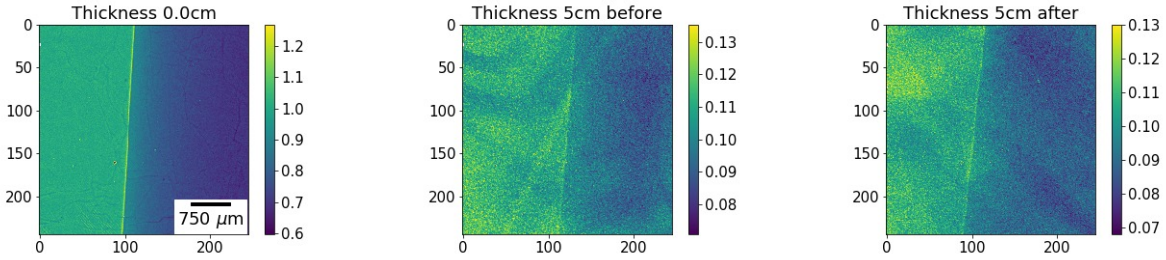

(a) (b) (c)

Figure 6: Edge enhancement measured with and without additional breast phantom slices. (a) Only signal; (b-c) signal propagating through additional 5 cm thick breast phantom placed before and after the signal, respectively.

The thickness dependent phase-contrast degradation has been determined by measuring the edge enhancement by placing additional PMMA thicknesses, 24 mm, 32.4 mm, 42 mm, 50.7 mm respectively, after the signal. Figures 7(a-b) show a comparison between the signal without any additional background thickness and the enhancement after photons propagation through additional 4.2 mm thick PMMA background. The dependence of the edge enhancement as function of the additional PMMA thickness is shown in Fig. 7(c). Within this thickness range plot shows a nearly linear trend. To note that after the propagation of the signal through additional 5 cm thick PMMA slab, the signal intensity is almost halved.

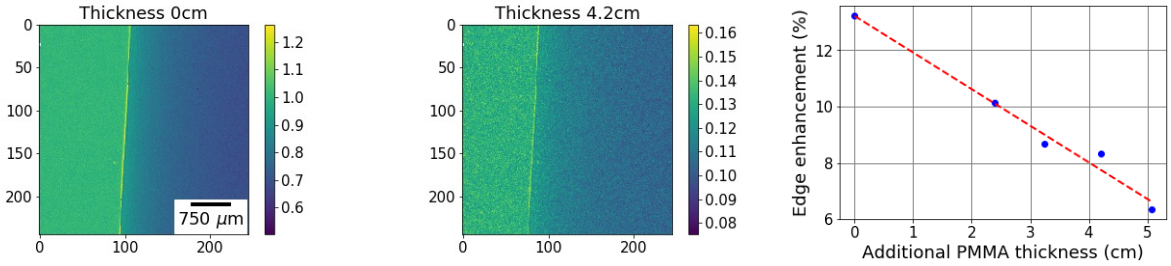

(a) (b) (c)

Figure 7: Decrease in the PMMA rod edge enhancement when photons further propagates through additional PMMA slices. (a) Only signal; (b) signal propagating through additional 4.2 cm thick PMMA slab placed after the signal. (c) Edge enhancement as function of the additional PMMA thickness.

Thickness dependent phase-contrast degradation has been determined for the coded aperture modality as well. Figure 8(a) shows the edge enhancement obtained in coded aperture PCI mode; Figs. 8(b-c) show the signal degradation after photons propagation through a 41 mm thick PMMA slab and a 40 mm thick breast phantom, respectively.

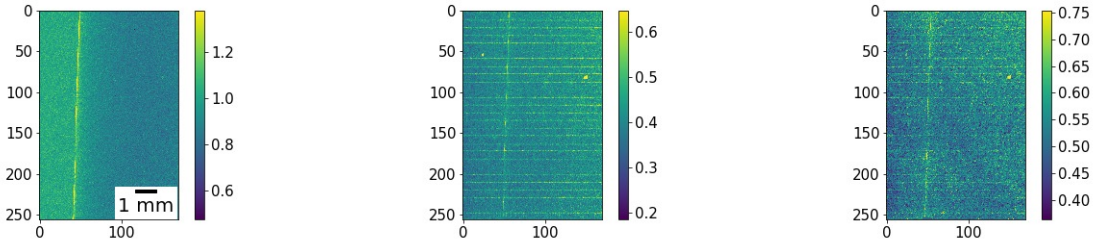

(a) (b) (c)

Figure 8: Decrease in the PMMA rod edge enhancement when signal further propagates through additional PMMA thickness. (a) Only signal; (b) signal after additional of 41 mm thick PMMA slab; (c) signal after additional 40 mm thick breast phantom. Images acquired in CA PCI geometry.

Thickness dependence of edge enhancement degradation in a coded aperture modality has found to be consistent to what is measured for free space propagation modality. Their comparison in shown in Fig. 9. Here edge enhancement values have been normalized by the one obtained when no additional PMMA background thickness was used. For this particular case, the slope of the global linear fit is approximately -0.1 cm^{-1}, meaning there is approximately a 10% decrease in the normalized edge enhancement for each additional centimeters of PMMA background placed after the signal. Perhaps, this last result provides an indication of the limit of applicability of the discussed PCI techniques. For this particular case, very low benefits from PCI are expected when a PMMA background larger than 10 cm is used.

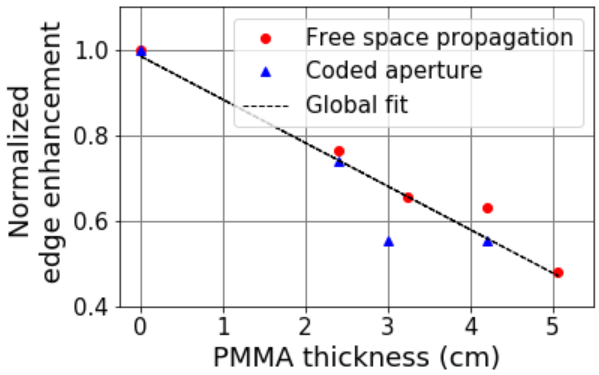

Figure 9: Decrease in the normalized edge enhancement as function of the additional PMMA thickness, for both free space propagation and coded aperture geometry. The slope of the global linear fit is approximately -0.1 cm^{-1}.

5. CONCLUSIONS

To summarize, a quantitative exploration of the impact of phase-contrast signal degradation due to its presence in a thick background has been performed. Experiments exploited free space propagation and coded aperture phase-contrast imaging techniques.

A preliminary optimization of experimental conditions were obtained for both techniques, in order to maximize phase contrast from the signal. The absolute edge enhancement values depends on a number of factors. These include materials properties, the shape of the object, the beam energy, the spatial and temporal coherence of the x-ray field, the particular experimental setting used etc.

Regardless of the particular phase-contrast technique used, the edge enhancement produced by the signal deteriorates when the signal is positioned within another thick sample. This situation is of particular interest, since it reflects a real clinical applications. Within the range of background thickness' used in this work, which are relevant for applications such as mammography, sufficient signal could be obtained. The phase enhanced signal was found to be not dependent on the signal position within the thicker background, but only on the overall object thickness. A linear decrease of the order of 10% for each additional centimeters of PMMA background placed after the signal was found. It can be concluded that for very thick specimen very low benefits from PCI techniques are expected. Further studies are required to understand implications of this on signal type and specific applications. However, within the range of thickness's (5cm) explored in this work, the phase contrast signal remains still sufficiently high to be clearly visible. Further work will explore implications of this in human observer's ability to detect these signals in a complex background.

6. ACKNOWLEDGEMENTS

This work was partially supported by funding from the US Department of Defense (DOD) Congressionally Directed Medical Research Program (CDMRP) Breakthrough Award BC151607 and the National Science Foundation CAREER Award 1652892.

REFERENCES

[1] Pogany, A., Gao, D., and Wilkins, S., "Contrast and resolution in imaging with a microfocus x-ray source," *Review of Scientific Instruments* **68**(7), 2774–2782 (1997).

[2] Gureyev, T., Mayo, S., Myers, D., Nesterets, Y., Paganin, D., Pogany, A., Stevenson, A., and Wilkins, S., "Refracting röntgens rays: propagation-based x-ray phase contrast for biomedical imaging," *Journal of Applied Physics* **105**(10), 102005 (2009).

[3] Nugent, K. A., "The measurement of phase through the propagation of intensity: an introduction," *Contemporary Physics* **52**(1), 55–69 (2011).
[4] Teague, M. R., "Deterministic phase retrieval: a Greens function solution," *JOSA* **73**(11), 1434–1441 (1983).
[5] Gureyev, T., Mayo, S., Wilkins, S., Paganin, D., and Stevenson, A., "Quantitative in-line phase-contrast imaging with multienergy x rays," *Physical Review Letters* **86**(25), 5827 (2001).
[6] Mayo, S., Miller, P., Wilkins, S., Davis, T., Gao, D., Gureyev, T., Paganin, D., Parry, D., Pogany, A., and Stevenson, A., "Quantitative X-ray projection microscopy: phase-contrast and multi-spectral imaging," *Journal of microscopy* **207**(2), 79–96 (2002).
[7] Wu, X. and Liu, H., "A general theoretical formalism for X-ray phase contrast imaging," *Journal of X-ray Science and Technology* **11**(1), 33–42 (2003).
[8] Wu, X. and Liu, H., "Phase-space formulation for phase-contrast x-ray imaging," *Applied optics* **44**(28), 5847–5854 (2005).
[9] Lewis, R., "Medical phase contrast x-ray imaging: current status and future prospects," *Physics in medicine and biology* **49**(16), 3573 (2004).
[10] Wilkins, S., Gureyev, T. E., Gao, D., Pogany, A., and Stevenson, A., "Phase-contrast imaging using polychromatic hard x-rays," *Nature* **384**(6607), 335 (1996).
[11] Olivo, A. and Speller, R., "A coded-aperture technique allowing x-ray phase contrast imaging with conventional sources," *Applied Physics Letters* **91**(7), 074106 (2007).
[12] Wu, X. and Liu, H., "Clinical implementation of x-ray phase-contrast imaging: Theoretical foundations and design considerations," *Medical physics* **30**(8), 2169–2179 (2003).
[13] Zhou, S.-A. and Brahme, A., "Development of phase-contrast X-ray imaging techniques and potential medical applications," *Physica Medica* **24**(3), 129–148 (2008).
[14] Olivo, A., Gkoumas, S., Endrizzi, M., Hagen, C., Szafraniec, M., Diemoz, P., Munro, P., Ignatyev, K., Johnson, B., Horrocks, J., et al., "Low-dose phase contrast mammography with conventional x-ray sources," *Medical physics* **40**(9) (2013).
[15] Das, M. and Liang, Z., "Approximated transport-of-intensity equation for coded-aperture x-ray phase-contrast imaging," *Optics letters* **39**(18), 5395–5398 (2014).
[16] Das, M. and Liang, Z., "Spectral x-ray phase contrast imaging for single-shot retrieval of absorption, phase, and differential-phase imagery," *Optics letters* **39**(21), 6343–6346 (2014).
[17] Gürsoy, D. and Das, M., "Single-step absorption and phase retrieval with polychromatic x rays using a spectral detector," *Optics letters* **38**(9), 1461–1463 (2013).
[18] Ballabriga, R., Alozy, J., Blaj, G., Campbell, M., Fiederle, M., Frojdh, E., Heijne, E., Llopart, X., Pichotka, M., Procz, S., et al., "The Medipix3RX: a high resolution, zero dead-time pixel detector readout chip allowing spectroscopic imaging," *Journal of Instrumentation* **8**(02), C02016 (2013).
[19] Ballabriga, R., Alozy, J., Campbell, M., Frojdh, E., Heijne, E., Koenig, T., Llopart, X., Marchal, J., Pennicard, D., Poikela, T., et al., "Review of hybrid pixel detector readout ASICs for spectroscopic X-ray imaging," *Journal of Instrumentation* **11**(01), P01007 (2016).
[20] Taguchi, K. and Iwanczyk, J. S., "Vision 20/20: Single photon counting x-ray detectors in medical imaging," *Medical physics* **40**(10) (2013).